Inorganic Chemistry

Article

pubs.acs.org/IC

Regioselectivity in Ligand Substitution Reactions on Diiron Complexes Governed by Nucleophilic and Electrophilic Ligand Properties

Ryan D. Bethel,[†] Danielle J. Crouthers,[†] Chung-Hung Hsieh,[§] Jason A. Denny,[†] Michael B. Hall,*[,†] and Marcetta Y. Darensbourg*[,†]

[†]Department of Chemistry, Texas A&M University, College Station, Texas 77843, United States

[§]Department of Chemistry, Tamkang University, Taiwan 25157

Supporting Information

ABSTRACT: The discovery of a diiron organometallic site in nature within the diiron hydrogenase, [FeFe]-H_2ase, active site has prompted revisits of the classic organometallic chemistry involving the Fe−Fe bond and bridging ligands, particularly of the (μ-SCH_2XCH_2S)[$Fe(CO)_3$]$_2$ and (μ-SCH_2XCH_2S)[$Fe(CO)_2L$]$_2$ (X = CH_2, NH; L = PMe_3, CN^-, and NHC's (NHC = N-heterocyclic carbene)), derived from CO/L exchange reactions. Through the synergy of synthetic chemistry and density functional theory computations, the regioselectivity of nucleophilic (PMe_3 or CN^-) and electrophilic (nitrosonium, NO^+) ligand substitution on the diiron dithiolate framework of the (μ-pdt)[$Fe(CO)_2$NHC][$Fe(CO)_3$] complex (pdt = propanedithiolate) reveals the electron density shifts in the diiron core of such complexes that mimic the [FeFe]-H_2ase active site. While CO substitution by PMe_3, followed by reaction with NO^+, produces (μ-pdt)(μ-CO)[Fe(NHC)(NO)][$Fe(CO)_2PMe_3$]$^+$, the alternate order of reagent addition produces the structural isomer (μ-pdt)[Fe(NHC)(NO)PMe_3][$Fe(CO)_3$]$^+$, illustrating how the nucleophile and electrophile choose the electron-poor metal and the electron-rich metal, respectively. Theoretical explorations of simpler analogues, (μ-pdt)[$Fe(CO)_2CN$][$Fe(CO)_3$]$^-$, (μ-pdt)[$Fe(CO)_3$]$_2$, and (μ-pdt)[$Fe(CO)_2NO$][$Fe(CO)_3$]$^+$, provide an explanation for the role that the electron-rich iron moiety plays in inducing the rotation of the electron-poor iron moiety to produce a bridging CO ligand, a key factor in stabilizing the electron-rich iron moiety and for support of the rotated structure as found in the enzyme active site.

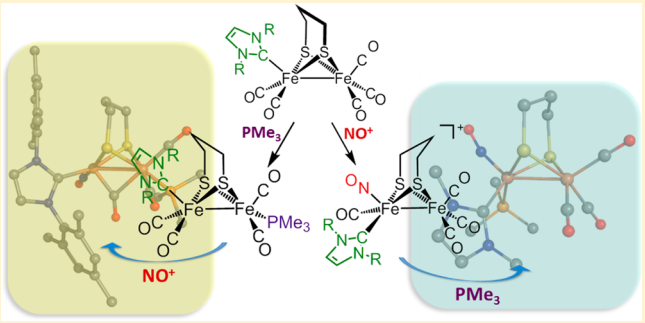

INTRODUCTION

The surprisingly simple iron carbonyl complex, (μ-pdt)[$Fe(CO)_3$]$_2$ (**1**), pdt = $-S(CH_2)_3S-$,[1] has a broad range of physical and chemical properties that have provided an understanding of the natural diiron catalytic site within diiron hydrogenase, [FeFe]-H_2ase. The structure of the [FeFe]-H_2ase active site, HydA, can be seen in Figure 1.[2] Although meager in contrast to the enzyme, the intrinsic activity of (μ-pdt)[$Fe(CO)_3$]$_2$ (**1**) as a solution electrocatalyst for proton reduction mimics the function of the enzyme, providing impetus for further development.[3] Modifications via the dithiolate bridging ligand and CO/L exchange have resulted in myriad, well-characterized diiron complexes.[4−6] Further adaptations including attachment into polymer supports,[7,8] inclusion into metal organic frameworks,[9] etc., have shown that the readily detectable diiron hexacarbonyl complex serves as prototype for development of solid-supported base metal molecular electrocatalysts in replacement of platinum in solar or fuel cells.

The validity of the (μ-adt)[$Fe(CO)_2CN$]$_2^{2-}$, adt = $-S(CH_2NHCH_2)S-$ or azadithiolate,[14] as a synthetic precursor to the diiron subsite as delivered to apo-[FeFe]-H_2ase has been demonstrated in recent studies that showed the dicyano derivative, (μ-adt)[$Fe(CO)_2CN$]$_2^{2-}$, generated by CN^-/CO exchange from (μ-adt)[$Fe(CO)_3$]$_2$, readily incorporates into the apo-[FeFe]-H_2ase lacking the 2Fe subsite.[10,11] According to various spectroscopies, the hybrid enzyme is identical in active site structure and achieves complete reactivity of the wild type enzyme (Figure 1).[10,11] Hence, the CN^-/CO substitution reactions of (μ-pdt)[$Fe(CO)_3$]$_2$, explored over a decade ago for their mechanistic impact,[15,16] become pertinent again as the full significance and possibility of even more organoiron units in biology are revealed through their presence in precursor proteins.

In fact, as the 2Fe subsite is incorporated into the HydA enzyme,[12,17] there is yet another substitution process when a cysteine attached to a 4Fe4S cluster displaces another CO, and anchors the 2Fe subsite, now containing three carbonyls and two cyanides, to the protein. A general question lies in nature's design of this collection of Fe, S, and diatomic ligands in the

Received: January 9, 2015
Published: March 13, 2015

DOI: 10.1021/acs.inorgchem.5b00072
Inorg. Chem. 2015, 54, 3523−3535

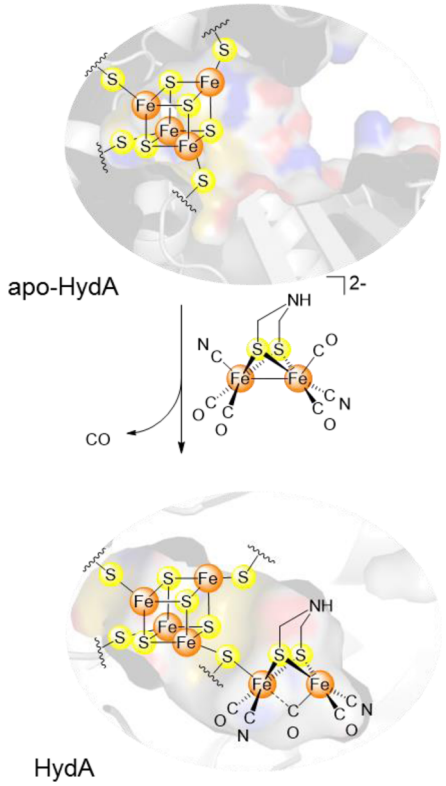

Figure 1. Ball-and-stick depiction of the insertion of the synthetic (μ-adt)$[Fe(CO)_2CN]_2^{2-}$ into the apo-[FeFe]H_2ase (apo-HydA) active site binding pocket, generating the fully functional enzyme (HydA).[10,11] The apo-HydA and HydA structures were generated using PyMol from the structures 3LX4 and 1HFE in the protein databank.[12,13]

finished enzyme and the particular arrangement that undoubtedly involves electron density flow between the attached 4Fe4S cluster and the terminal iron site where hydrogen activity occurs.[18] We and others address these issues by exploring ligand effects on charge distribution and reactivity of synthetic analogues.

Equations 1 and 2 within Figure 2 summarize nucleophilic (Nuc:) substitution reactions which for CN^- and PMe_3 as entering ligands displace CO ligands on alternate irons, as expected for optimal charge distribution within the complexes.[4,19] The most common result of an electrophilic attack ($Elec^+ = H^+$ or SR^+) on the diiron complexes is the formation of the bridging (μ-Elec)(μ-SRS)$[Fe(CO)_2L]_2^+$ complex (eq 3, Figure 2).[20,21] However, the kinetic product of electrophilic attack, according to theory and corroborated by experiment, is a terminal Fe-H or Fe-SR (from H^+ and SR^+, respectively, as electrophiles).[21,22] A less common site of electrophilic attack is the sulfur of the bridging thiolate. The formation of $[(\mu\text{-SRS}(\text{-Elec}))[Fe(CO)_2L]_2]^{n+}$ has been observed in the cases of addition of Et^+ or O atoms;[19,23] initial S-based reactivity has also been implicated as an intermediate step in protonation, ultimately leading to a (μ-H)Fe_2 species.[24]

Several studies have addressed the use of NO^+ as an electrophile that proceeds with isoelectronic CO exchange.[25−27] The strongly electron-withdrawing NO^+ ligand significantly modifies the electronic environment and structures of products from such exchange, replicating the electronic asymmetry of the mixed-valent Fe^IFe^{II} complexes.[25] In the case of CO/NO^+ exchange in (μ-pdt)$[Fe(CO)_2PMe_3]_2$, the asymmetry of the product, (μ-pdt)$[Fe(CO)_2PMe_3][Fe(CO)(NO)PMe_3]^+$, results in increased Lewis acidity of the substituted iron and susceptibility to further CO/L substitution.[25] In the solid state, this complex exists as a mixture of structural isomers, one in quasi C_{2v} symmetry and the other approaching the geometry of a "rotated" structure, containing an inverted square pyramid with a bridging CO group, analogous to the 2Fe subsite of the [FeFe]-H_2ase active site.[25] With steric bulk at the bridgehead of the μ-SRS unit, we have seen that the analogous (μ-dmpdt)$[Fe(CO)_2PMe_3]_2$ and (μ-depdt)$[Fe(CO)_2PMe_3]_2$ complexes (dmpdt = $-S(CH_2C(CH_3)_2CH_2)S-$; depdt = $-S(CH_2C(CH_2CH_3)_2CH_2)S-$) undergo NO^+/CO substitution to yield bridging-CO, rotated structures with no complications from isomers.[26] The resultant (μ-depdt)- or (μ-dmpdt)(μ-CO)$[Fe(PMe_3)NO][Fe(CO)_2PMe_3]^+$ complexes are isostructural with the one-electron oxidized, paramagnetic, mixed-valent (μ-dmpdt)(μ-CO)-

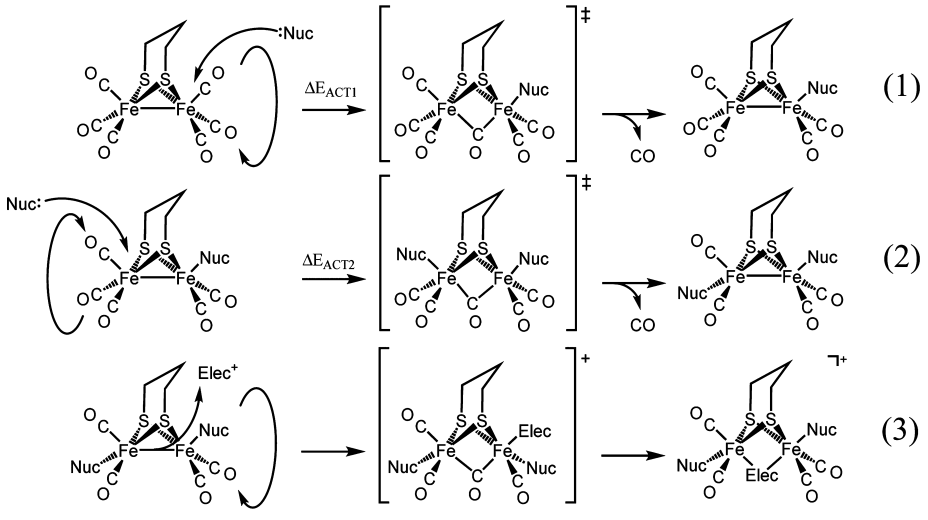

Figure 2. Mechanisms of nucleophilic CO substitution (eqs 1 and 2), where the activation energy for CO substitution for the first incoming ligand (ΔE_{ACT1}) is greater than that of the second (ΔE_{ACT2}) if the ligands are CN^-, whereas the reverse ($\Delta E_{ACT1} < \Delta E_{ACT2}$) is true for PMe_3.[4,19] The oxidative addition of electrophiles such as H^+ and MeS^+ to the doubly substituted complex (eq 3) results in a bridging ligand with no loss of CO.[21,22]

DOI: 10.1021/acs.inorgchem.5b00072
Inorg. Chem. 2015, 54, 3523−3535

$[Fe^{I}(CO)PMe_3][Fe^{II}(CO)_2PMe_3]^+$.[26] Mössbauer and EPR spectroscopies and computational studies supported the oxidation state assignment in the rotated structure. The diamagnetism of the NO analogue suggested that the diiron core consisted of a spin-coupled d^7-Fe^{I}-NO•, denoted as $\{Fe(NO)\}^8$ by the Enemark–Feltham notation,[28] and an Fe^{II}. Nevertheless, other possibilities exist for electronic assignment in such an $\{FeFe(NO)\}^{14}$ arrangement.

An alternate approach of generating the rotated structures is to introduce steric bulk into the substitutent ligand rather than the dithiolate bridge. The N-heterocyclic carbene ligand, IMes, 1,3-bis(2,4,6-trimethylphenyl)imidazole-2-ylidene, met this criterion in the one-electron oxidized, mixed-valent (μ-pdt)(μ-CO)$[Fe^{I}(CO)IMes][Fe^{II}(CO)_2PMe_3]^+$ complex.[29] Our effort to explore the nitrosylated NHC complexes for the possibility of rotated structures was the initial impetus for studies in the following report. Herein, we describe experimental and computational investigations into NO^+/CO exchange in NHC and PMe_3 substituted derivatives of (μ-pdt)$[Fe(CO)_3]_2$, where NHC designates the N-heterocyclic carbenes IMes and IMe = 1,3-dimethylimidazole-2-ylidene, as strong sigma donors. An unexpected benefit of the synthetic effort is that the subtle differences in donor abilities of the NHC vs PMe_3 ligands had dramatic influence on substitution pattern and product geometries. With the aid of theory, these differences are interpreted as the result of charge delocalization via an asymmetric Fe(μ-CO)Fe interaction wherein the bridging carbonyl acceptor arises from the more electron-deficient iron in the "rotated" isomer configuration.

EXPERIMENTAL SECTION

General Procedures and Physical Methods. All reactions and operations were carried out on a double manifold Schlenk vacuum line, under a N_2 atmosphere; an Ar-filled glovebox was used in the manipulation and storage of air-sensitive compounds. Solvents were purified on a MBraun Manual Solvent Purification System, packed with Alcoa F200 activated alumina desiccant. The purified solvents were stored under a N_2 atmosphere prior to use. The N-heterocyclic carbenes, IMe = 1,3-dimethylimidazole-2-ylidene and IMes = 1,3-bis(2,4,6-trimethylphenyl)imidazole-2-ylidene, were obtained by deprotonation of the imidazolium salts (IMe^+I^- and $IMes^+Cl^-$, respectively), which were synthesized according to literature procedures.[30,31] The known complexes, (μ-pdt)$[Fe(CO)_3]_2$ (pdt = 1,3-propanedithiolate),[1] **1**; (μ-pdt)$[Fe(CO)_2IMe][Fe(CO)_3]$,[32] **1-IMe**; (μ-pdt)$][Fe(CO)_2IMes][Fe(CO)_3]$,[33] **1-IMes**; ($\mu$-pdt)$][Fe(CO)_2IMe][Fe(CO)_2PMe_3]$,[34] **5-IMe**; and ($\mu$-pdt)$][Fe(CO)_2IMes][Fe(CO)_2PMe_3]$,[29] **5-IMes**, were prepared according to literature procedures. The following materials were purchased as reagent grade and used without further purification: trimethylphosphine (PMe_3), nitrosonium tetrafluoroborate ($[NO]^+[BF_4]^-$), tetrabutylammonium cyanide ($[Bu_4N]^+[CN]^-$), chloroform-*d*, methylene chloride-d_2, and 1,4,7,10,13,16-hexaoxacyclooctadecane (18-crown-6).

Solution infrared spectroscopy was carried out on a Bruker Tensor 37 FTIR spectrometer using a 0.2 mm CaF_2 sealed cell for all measurements. Mass spectrometry (ESI-MS) was performed by the Laboratory for Biological Mass Spectrometry at Texas A&M University. Elemental analyses were performed by Atlantic Microlab, Inc., Norcross, Georgia, USA. Room-temperature ^1H and ^{13}C NMR spectra were obtained using a Mercury 300 MHz NMR spectrometer; ^{31}P NMR spectra were obtained using an Inova 300 MHz NMR Spectrometer. Variable-temperature ^{13}C NMR spectra were obtained on a Unity+ 500 MHz NMR instrument operating between 0 and 30 °C. Exchange of $^{12}CO/^{13}CO$ was monitored by *in situ* infrared spectroscopy, using a Mettler Toledo iC10 ReactIR with an AgX fiber conduit probe having a SiComp ATR crystal. Irradiation of samples was carried out using a Newport Oriel Apex Illuminator 100 W Hg UV lamp and Pyrex vessels. Cyclic voltammograms were recorded on a BAS-100A electrochemical analyzer; details and scans are in the Supporting Information.

X-ray Structure Analysis. X-ray diffraction data for all complexes were obtained at low temperature (110/150 K) on a Bruker Apex-II CCD based diffractometer (Texas A&M University) (Mo sealed X-ray tube, Kα = 0.71073 Å). A crystalline sample was coated in mineral oil, affixed to a Nylon loop, and placed under streaming N_2. The space groups were determined by systematic absences and intensity statistics, and structures were solved by direct methods and refined by full-matrix least-squares on F^2. Anisotropic displacement parameters were employed for all non-hydrogen atoms; H atoms were placed at idealized positions and refined with fixed isotropic displacement parameters. The following programs were used: cell refinement, data collection, data reduction, APEX2;[35] absorption correction, SADABS;[36] structure solutions, SHELXS-97;[37] and structure refinement, SHELXL-97.[38] The final data presentation and structure plots were generated in X-Seed Version 2.0[39] and Mercury version 2.3.[40] CIF files were prepared for publication using WinGX[41] and its included programs.

Synthesis of (μ-pdt)[Fe(IMe)(NO)(CO)][Fe(CO)$_3$]$^+$[BF$_4$]$^-$ (2-IMe). Complex **2-IMe** was prepared from a solution of **1-IMe**, (μ-pdt)$[Fe(CO)_2IMe][Fe(CO)_3]$, (0.44 g, 0.97 mmol) dissolved in 40 mL of CH_2Cl_2. This red solution was chilled to 0 °C in an ice water bath. A second solution of $[NO]^+[BF_4]^-$ (0.11 g, 0.97 mmol) and 18-crown-6 (0.26 g, 0.97 mmol) was prepared in 20 mL of CH_2Cl_2 in an ice water bath. This pale yellow solution was magnetically stirred for up to 30 min to allow for complete dissolution of the nitrosonium salt, at which time it was slowly added to the solution of **1-IMe**. The reaction was monitored by solution IR until formation of product ceased, approximately 30 min. The resulting dark red solution was anaerobically filtered through Celite. The **2-IMe** product was precipitated on addition of hexanes. Repeated washes with hexanes and diethyl ether at 0 °C resulted in pure product. Crystals of X-ray quality were obtained by layering a solution of **2-IMe** in CH_2Cl_2/Et_2O at −25 °C. Yield: 0.25 g (52%). IR (CH_2Cl_2) ν(CO): 2085(s), 2058(s), 2018(s); ν(NO): 1809(s); C-13 NMR (CD_2Cl_2), CO region, 0 °C: 207.1, 206.2, 204.0, 202.9 (1:1:1:1). Anal. Calcd for $C_{12}H_{14}BF_4Fe_2N_3O_5S_2$: C, 26.6; H, 2.60; N, 7.74. Found: C, 27.2; H, 3.11; N, 7.10. ESI-MS+ Calcd for parent ion (μ-pdt) [Fe(IMe)(NO)(CO)][Fe(CO)$_3$]$^+$, $C_{12}H_{14}Fe_2N_3O_5S_2$: 455.91. Found: 455.92.

Synthesis of (μ-pdt)[Fe(IMes)(NO)(CO)][Fe(CO)$_3$]$^+$[BF$_4$]$^-$ (2-IMes). In a similar manner to **2-IMe** above, complex **2-IMes** was prepared from a solution of **1-IMes**, (μ-pdt)$[Fe(CO)_2(IMes)][Fe(CO)_3]$, (0.20 g, 0.30 mmol) dissolved in 40 mL of CH_2Cl_2, cooled, and reacted with a similarly chilled CH_2Cl_2 solution of $[NO]^+[BF_4]^-$ (0.035 g, 0.30 mmol) and 18-crown-6 (0.080 g, 0.30 mmol). Isolation, purification, and crystallization were as described above. Yield: 0.083 g (35%). IR (CH_2Cl_2) ν(CO): 2085(s), 2039(m), 2025(m); ν(NO): 1792(m). Anal. Calcd $C_{28}H_{30}BF_4Fe_2N_3O_5S_2$: C, 43.8; H, 4.03; N, 5.59. Found: C, 43.9; H, 4.10; N, 5.39. ESI-MS+ Calcd for parent ion (μ-pdt)[Fe(IMes)(NO)(CO)][Fe(CO)$_3$]$^+$, $C_{12}H_{14}Fe_2N_3O_5S_2$: 644.03. Found: 644.02.

Synthesis of (μ-pdt)[Fe(IMe)(NO)(CN)][Fe(CO)$_3$] (3-IMe). Complex **3-IMe** was prepared from **2-IMe** (0.20 g, 0.34 mmol), dissolved in 30 mL of tetrahydrofuran (THF). This red solution was chilled to 0 °C, and then transferred via cannula to a suspension of 0.047 g (0.30 mmol) $[Et_4N]^+[CN]^-$ in 10 mL of THF at 0 °C. The reaction was monitored by solution IR until formation of **3-IMe** ceased, after approximately 3 h. The resulting light red solution was filtered through Celite, removing any unreacted $[Et_4N]^+[CN]^-$. The product, **3-IMe**, was isolated from unreacted starting material by slow addition of Et_2O, precipitating any remaining unreacted cyanide salts or **2-IMe**. The solution was filtered and solvent was removed *in vacuo*, yielding a red solid which was washed with a 10:1 mixture of hexanes/Et_2O; purity was monitored by IR spectroscopy in the diatomic ligand region (2200–1600 cm^{-1}). Crystals of X-ray quality were obtained by layering **3-IMe** in CH_2Cl_2/hexanes/Et_2O at −25 °C. Yield: 0.050 g (38%). IR (CH_2Cl_2) ν(CN): 2112(vw); ν(CO): 2054(s), 1988(s); ν(NO): 1755(m). ESI-MS+ Calcd for parent plus the Et_4N^+ ion (μ-

DOI: 10.1021/acs.inorgchem.5b00072
Inorg. Chem. 2015, 54, 3523–3535

Scheme 1. Synthetic Routes toward Symmetric and Dissymmetric (μ-pdt)[FeFe] Complexes

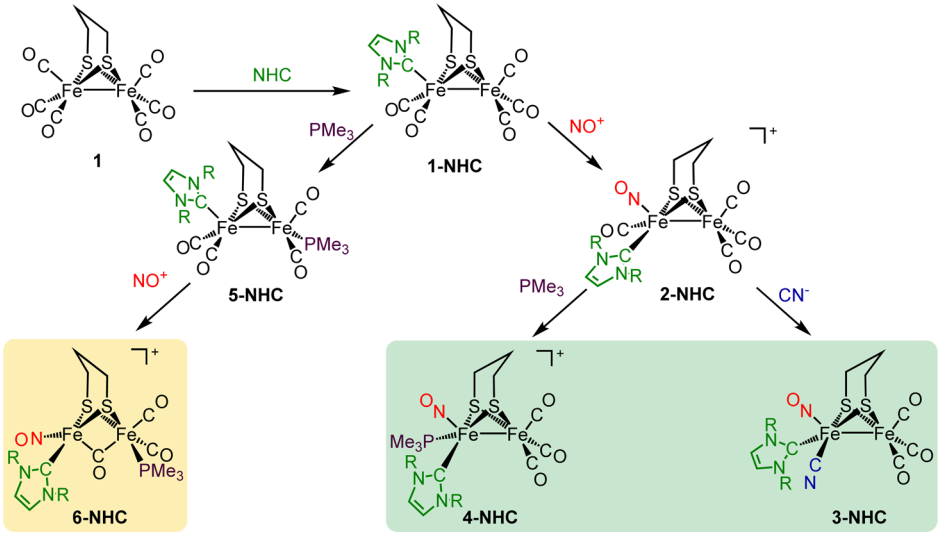

Table 1. Experimental CH_2Cl_2 Solution Vibrational Frequencies of Diatomic Ligands of Relevant (pdt)[FeFe] Complexes

complexes	vibrational frequencies[a]
(μ-pdt)[Fe(CO)$_3$]$_2$, **1**	2072(m), 2037(s), 1990(s)[1]
(μ-pdt)[Fe(CO)$_2$IMe][Fe(CO)$_3$], **1-IMe**	2035(m), 1971(s), 1952(m), 1915(m)[32]
(μ-pdt)[Fe(CO)$_2$IMes][Fe(CO)$_3$], **1-IMes**	2035(m), 1969(s), 1947(w), 1916(w)[33]
(μ-pdt)[Fe(IMe)(NO)(CO)][Fe(CO)$_3$]$^+$BF$_4^-$, **2-IMe**	2085(s), 2058(s), 2018(s), [1809(s)][b]
(μ-pdt)[Fe(IMes)(CO)(NO)][Fe(CO)$_3$]$^+$BF$_4^-$, **2-IMes**	2085(s), 2039(m), 2024(m), [1792(m)][b]
(μ-pdt)[Fe(IMe)(NO)(CN)][Fe(CO)$_3$], **3-IMe**	{2112(vw)}, 2054(s), 1988(s), [1755(m)][b]
(μ-pdt)[Fe(IMe)(NO)PMe$_3$][Fe(CO)$_3$]$^+$BF$_4^-$, **4-IMe**	2061(s), 1996(s), [1759(m)][b]
(μ-pdt)[Fe(CO)$_2$IMe][Fe(CO)$_2$PMe$_3$], **5-IMe**	1974(s), 1934(s), 1898(m), 1884(sh)[34]
(μ-pdt)[Fe(CO)$_2$IMes][Fe(CO)$_2$PMe$_3$], **5-IMes**	1972(m), 1933(s), 1896(m), 1881(sh)[29]
(μ-pdt)(μ-CO)[Fe(IMe)(CO)][Fe(CO)$_2$PMe$_3$]$^+$PF$_6^-$, **5-IMe**$^+$	2036(s), 2005(s), 1981(s), 1929(w)[34]
(μ-pdt)(μ-CO)[Fe(IMes)(CO)][Fe(CO)$_2$PMe$_3$]$^+$PF$_6^-$, **5-IMes**$^+$	2036(s), 1997(s), 1987(sh), 1861(w)[29]
(μ-pdt)(μ-CO)[Fe(IMe)(NO)][Fe(CO)$_2$PMe$_3$]$^+$BF$_4^-$, **6-IMe**	2031(s), 1977(m), [1784(m)][b]
(μ-pdt)(μ-CO)[Fe(IMes)(NO)][Fe(CO)$_2$PMe$_3$]$^+$BF$_4^-$, **6-IMes**	2035(m), 1996(s), [1782(m)][b]

[a]Values in brackets, [ ], and in braces, { }, are for (NO) and (CN), respectively. [b]This work.

pdt)[Fe(IMe)(NO)(CN)][Fe(CO)$_3$][N(C$_2$H$_5$)$_4$]$^+$, $C_{20}H_{34}Fe_2N_5O_4S_2$: 584.08. Found: 584.08.

Synthesis of (μ-pdt)[Fe(IMe)(NO)PMe$_3$][Fe(CO)$_3$]$^+$[BF$_4$]$^-$ (4-IMe). Complex **4-IMe** was prepared from a solution of **2-IMe** (0.20 g, 0.34 mmol) in 40 mL of CH_2Cl_2. The solution was chilled in an ice water bath, and 35 μL (0.34 mmol) of PMe_3 was added via microsyringe. The reaction was monitored by IR spectroscopy, noting complete conversion to product in less than 15 min. The product, **4-IMe**, was filtered through Celite, precipitated with addition of hexanes, and washed several times with Et_2O at 0 °C. Crystals of X-ray quality were obtained by layering **4-IMe** in CH_2Cl_2/Et_2O at −25 °C. Yield: 0.15 g (69%). IR (CH_2Cl_2) ν(CO): 2062(s), 1996(s); ν(NO): 1758(m); C-13 NMR (CD_2Cl_2), CO region, 0 °C: 207.4, 206.9, 206.0 (1:1:1). Anal. Calcd $C_{14}H_{25}BF_4Fe_2N_3O_5S_2P_1$: C, 27.4; H, 3.95; N, 6.90. Found: C, 27.6; H, 4.14; N, 6.90. ESI-MS+ Calcd for parent ion (μ-pdt)[Fe(IMe)(NO)PMe$_3$][Fe(CO)$_3$]$^+$, $C_{14}H_{23}Fe_2N_4O_4S_2P_1$: 503.96. Found: 503.94. See the Supporting Information file for cyclic voltammographic scans (Figure S1).

Syntheses of (μ-pdt)(μ-CO)[Fe(IMe)(NO)][Fe(CO)$_2$PMe$_3$]$^+$[BF$_4$]$^-$ (6-IMe) and (μ-pdt)(μ-CO)[Fe(IMes)(NO)][Fe(CO)$_2$PMe$_3$]$^+$[BF$_4$]$^-$ (6-IMes). Complexes **6-IMe** and **6-IMes** were prepared from solutions of **5-IMe** (0.20 g, 0.37 mmol) and **5-IMes** (0.20 g, 0.28 mmol), respectively, dissolved in 40 mL of CH_2Cl_2. These red solutions were chilled to 0 °C, and then transferred via cannula to suspensions of 0.043 g (0.37 mmol) and 0.033 g (0.28 mmol) of NO$^+$BF$_4^-$, respectively, in 40 mL of CH_2Cl_2 at 0 °C. The reactions were monitored by IR spectroscopy until formation of product ceased, approximately 3 h for both reactions. Similarly colored reddish brown solutions were obtained for both reactions. Each solution was filtered through Celite and the red solids, **6-IMe** and **6-IMes**, were obtained on precipitation with hexanes, and purified by repeated Et_2O washes until no starting material (**5-IMe** and **5-IMes**, respectively) could be observed in the IR spectrum. Characterization of these complexes was limited to infrared spectroscopy, although crystals of X-ray quality for **6-IMes** were obtained by layering a solution **6-IMes** in CH_2Cl_2/Et_2O at −25 °C. **6-IMe**: Yield: 0.054 g (23%). IR (CH_2Cl_2) ν(CO): 2031(s), 1977(m); ν(NO): 1784(m). **6-IMes**: Yield: 0.048 g (21%). IR (CH_2Cl_2) ν(CO): 2035(m), 1996(s); ν(NO): 1782(m).

Preparation of ^{13}CO-Labeled 2-IMe. Illuminating a solution of 0.50 g (1.3 mmol) of complex **1**, dissolved in hexanes, for 5 h while sealed under a ^{13}CO atmosphere produced a sufficiently enriched source of **1** for ^{13}C NMR studies. This solution was filtered through a plug of silica gel, and the uniformly ^{13}CO enriched **2-IMe** was synthesized from **1** by the methods described above. Selectively enriched **2-IMe** was produced by placing a sample of 0.10 g (0.24 mmol) of **2-IMe** dissolved in ∼10 mL of CH_2Cl_2, under an atmosphere of ^{13}CO for 2 h. This reaction was performed in a 100 mL flask, leaving 90 mL (4.0 mmol) of headspace to be filled with ^{13}CO(g) at 1 atm. The solution of selectively enriched product was filtered through a plug of Celite and dried at 0 °C. In order to examine the relative rates of CO exchange of the two Fe(CO)$_x$ moieties, aliquots were removed and flash-frozen under N_2 at the following time points: 0, 10, 20, 30, and 120 min.

DOI: 10.1021/acs.inorgchem.5b00072
Inorg. Chem. 2015, 54, 3523−3535

Computational Methodology. Geometry and frequency calculations were performed with the Gaussian 09[42] suite of programs in the gas-phase with the B3LYP functional[43−45] and the 6-311+G(d,p) basis set[46,47] on all atoms. Crystallographic coordinates were used as starting geometries for optimizations of the ground state structures. Optimizations of the isomeric forms of each complex used the ground state bond angles and distances of each ligand as starting positions. Enthalpy and Gibbs free energy corrections to the electronic energy of all stable geometries were calculated at 298.15 K by Gaussian. All relative free energies were compared to the initial optimized structure based on the crystallographic coordinates. Ground state geometries had no imaginary vibrational modes, while transition states were located with a single imaginary mode. The Ampac Graphical User Interface (AGUI) program[48] was used to extract geometric data.

RESULTS AND DISCUSSION

Synthetic Routes to Symmetric and Asymmetric [FeFe]-H_2ase Model Complexes. The synthesis of (μ-pdt)[Fe(CO)$_2$NHC][Fe(CO)$_3$], **1-NHC**, where NHC = IMe, IMes, etc., from (μ-pdt)[Fe(CO)$_3$]$_2$ has been reliably established.[32,33] The well-characterized complexes **1-IMe** and **1-IMes** were chosen for the current study for their ease of purification as well as their stability. The IMe and IMes ligands have very similar donor properties with considerably different steric bulk. Scheme 1 outlines the derivatives of **1-NHC** that were obtained and characterized in this study; note that **6-NHC** and **4-NHC** are isomers achieved by alternate order of reagent addition. The stick drawings of products are represented in the geometries established by X-ray diffraction analysis, *vide infra*. The ν(CO) and ν(NO) IR spectroscopic signals were used to monitor and identify all compounds of this study (Table 1). All complexes in this study are diamagnetic.

Synthesis of (μ-pdt)(μ-CO)[Fe(IMe)(NO)][Fe(CO)$_2$PMe$_3$]$^+$BF$_4^-$, 6-IMe, and (μ-pdt)(μ-CO)[Fe(IMes)(NO)][Fe(CO)$_2$PMe$_3$]$^+$BF$_4^-$, 6-IMes. The reaction of either **1-IMe** or **1-IMes** with PMe$_3$ yields the (μ-pdt)[Fe(CO)$_2$IMe][Fe(CO)$_2$PMe$_3$] (**5-IMe**) or (μ-pdt)[Fe(CO)$_2$IMes][Fe(CO)$_2$PMe$_3$] (**5-IMes**) complexes with nearly symmetric electron density on the irons.[29,34] The one-electron oxidation of **5-IMes** produces the mixed-valent Fe^{I}Fe^{II} complex, (μ-pdt)(μ-CO)[Fe(CO)IMes][Fe(CO)$_2$PMe$_3$]$^+$PF$_6^-$ (**5-IMes**$^+$), that is a "rotated" [FeFe]-H_2ase active site model, containing a bridging carbonyl ligand and a terminal open site.[29] The isoelectronic ligand exchange of NO$^+$ for CO acts as a one-electron internal oxidant, as established for (μ-dmpdt)(μ-CO)[Fe(NO)PMe$_3$][Fe(CO)$_2$PMe$_3$]$^+$BF$_4^-$.[26] Likewise, on addition of NO$^+$ to **5-IMe** or **5-IMes**, in CH$_2$Cl$_2$ at 0 °C, the NO$^+$/CO exchange products, **6-IMe** or **6-IMes**, were isolated. The structure of **6-IMes** was determined by X-ray crystallography, *vide infra*, to be "rotated", i.e., the (pdt)Fe(IMes)(CO)(NO) square pyramid is rotated by 180° from the neutral Fe^{I}Fe^{I} isomer, such that the apical ligand, now the CO, is in a bridging position between the two iron atoms. Thus, **6-IMes**, (μ-pdt)(μ-CO)[Fe(IMes)(NO)][Fe(CO)$_2$PMe$_3$]$^+$BF$_4^-$, is isostructural with **5-IMes**$^+$, but with one CO replaced by an NO$^+$. As was seen with **5-IMe**$^+$,[34] the use of the less bulky IMe ligand yields a product spectroscopically similar to its IMes substituted counterpart that is assigned to (μ-pdt)(μ-CO)[Fe(IMe)(NO)][Fe(CO)$_2$PMe$_3$]$^+$BF$_4^-$, **6-IMe**; however, it has not yet been crystallized. [Note: An argument may be made, based on the equivocal crystallographic data, that the bridging diatomic ligand is NO rather than CO. However, the assignment of μ-CO is supported by FT IR spectroscopy that indicates an unambiguous terminal NO at 1782 cm^{-1}.]

Synthesis of (μ-pdt)[Fe(IMe)(NO)(CO)][Fe(CO)$_3$]$^+$BF$_4^-$, 2-IMe, and (μ-pdt)[Fe(IMes)(NO)(CO)][Fe(CO)$_3$]$^+$BF$_4^-$, 2-IMes. The addition of NO$^+$ to **1-IMe** or **1-IMes** was carried out at 0 °C to impede decomposition of the nitrosylated products, **2-IMe** or **2-IMes**, which occurs within minutes on warming solutions to 22 °C. Exposure to air also results in the rapid decomposition of solutions of **2-IMe** and **2-IMes**. The anerobic decomposition of **2-IMe** is retarded by replacement of the inert atmosphere with CO(g). In addition, the degradation is slower when the syntheses of **2-IMe** or **2-IMes** are carried out in CH$_2$Cl$_2$. However, as the [NO]$^+$[BF$_4$]$^-$ salt is largely insoluble in this solvent, the heterogeneous conditions, even on a small scale (~0.10 g), may take hours to reach 50% completion, greatly increasing the byproducts and the need for purification, thereby drastically reducing the yield. As reported by Connelly and Geiger,[49] the cyclic ether, 18-crown-6, solubilizes [NO]$^+$[BF$_4$]$^-$ in CH$_2$Cl$_2$,[50] even with a substoichiometric amount (10 mol %), and the reaction with **1-IMe** and **1-IMes** reaches completion in minutes at 0 °C, yielding the pure product. The products, **2-IMe** and **2-IMes**, are inert to further NO$^+$/CO exchange; both may be stored as solid powders under an inert atmosphere for days at −25 °C without decomposition.

Synthesis of (μ-pdt)[Fe(IMe)(NO)(CN)][Fe(CO)$_3$], 3-IMe, and (μ-pdt)[Fe(IMe)(NO)PMe$_3$][Fe(CO)$_3$]$^+$BF$_4^-$, 4-IMe. The addition of cyanide or trimethylphosphine to **2-IMe** proceeds with displacement of CO and results in one fully substituted iron, while the other remains as an intact [Fe(CO)$_3$] unit. The addition of CN$^-$ takes place in THF at 0 °C, where the cyanide salt is sparingly soluble, and the reaction is slow. Although CH$_2$Cl$_2$ may be used to generate the product, (μ-pdt)[Fe(IMe)(NO)(CN)][Fe(CO)$_3$], **3-IMe**, the reaction in THF produces a cleaner IR spectrum, indicating a single product is present in high purity. The addition of PMe$_3$ to **2-IMe** takes place at 0 °C in CH$_2$Cl$_2$. The reaction is complete within minutes, with a nearly quantitative yield of the product, (μ-pdt)[Fe(IMe)(NO)PMe$_3$][Fe(CO)$_3$]$^+$BF$_4^-$, **4-IMe**. Addition of excess PMe$_3$ does not result in a second CO substitution at this temperature. In contrast to its precursor, **2-IMe**, and its analogue, **3-IMe**, the **4-IMe** complex is relatively stable and may be handled as a solid under air and at ambient temperatures for several hours without decomposition. Note, as indicated in Scheme 1, that 6-NHC and 4-NHC are isomers; however, they were not observed to interconvert. The 6-NHC is thermally unstable and 4-NHC retains its configuration when exposed to heat or light.

Infrared Spectroscopy. The ν(CO) and ν(NO) IR values of relevant (μ-pdt)[FeFe] complexes are presented in Table 1, and the IR spectra in the diatomic region of **1**, **1-IMe**, **2-IMe**, **3-IMe**, and **4-IMe** are presented in Figure 3. As expected, the ν(CO) IR bands of **1** are shifted to lower frequencies on substitution of a CO ligand by the good donor ligands IMe or IMes. Differences in the pattern and position of ν(CO) bands between the two NHC derivatives, **1-IMe** and **1-IMes**, are minor (Figure S2, Supporting Information). The products resulting from addition of [NO]$^+$[BF$_4$]$^-$ have ν(CO) shifts to higher values and a dramatic change in the pattern of CO stretches (Figure 3). In addition to the three ν(CO) bands, a ν(NO) band appears at 1809 cm^{-1} (**2-IMe**) and 1792 cm^{-1} (**2-IMes**). Unlike the minor differences in the spectra of **1-IMe** and **1-IMes**, the respective nitrosylated species are distinct (Figure S2). Although both **2-IMe** and **2-IMes** display an intense, sharp ν(CO) band at 2085 cm^{-1}, the other two carbonyl bands of **2-IMe** are equally intense with minimal

DOI: 10.1021/acs.inorgchem.5b00072
Inorg. Chem. 2015, 54, 3523−3535

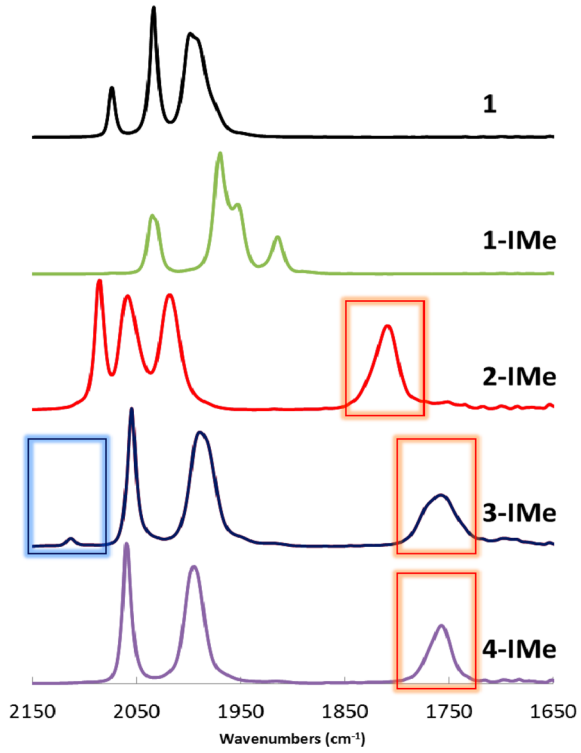

Figure 3. Solution (CH_2Cl_2) IR spectra for complexes **1**, **1-IMe**, **2-IMe**, **3-IMe**, and **4-IMe** in diatomic ligand region. The CN band of **3-IMe** is marked with a blue box; the NO bands of **2-IMe**, **3-IMe**, and **4-IMe** are marked with red boxes.

overlap, being some 40 cm^{-1} separated at 2058 and 2018 cm^{-1}. In contrast, the two lower ν(CO) bands of **2-IMes** are less intense and overlap more, with only 14 cm^{-1} separation at 2039 and 2025 cm^{-1}.

Addition of donor ligands, CN^- or PMe_3, to **2-IMe** results in a shift of ν(CO) and ν(NO) bands to lower frequencies. If cyanide is utilized, a new ν(CN) band appears at 2112 cm^{-1} (Figure 3). The ν(CO) bands for this complex, **3-IMe**, shift to 2054 and 1988 cm^{-1}, taking on the two-band pattern similar to that found for the C_{3v} structure as found in the piano stool complex $(\eta^5\text{-}C_5H_5)Fe(CO)_3^+$.[51]

The same pattern is seen in the ν(CO) bands of complex **4-IMe**, which contains a PMe_3 ligand rather than CN^-. Consistent with the relative donor properties, CN^- > PMe_3, the ν(CO) bands of the PMe_3-containing complex, **4-IMe**, are slightly higher in frequency, at 2061 and 1996 cm^{-1}. The ν(NO) band of **4-IMe** is slightly higher than that of **3-IMe** at 1759 and 1755 cm^{-1}, respectively.

The CH_2Cl_2 solution IR spectrum of **6-IMes** in the diatomic region shows two absorptions for ν(CO) at positions similar to those of $(\mu\text{-dmpdt})(\mu\text{-CO})[Fe(NO)PMe_3][Fe(CO)_2\text{-}PMe_3]^+$.[26] The ν(NO) band at 1782 cm^{-1} for **6-IMes** matches that for the bis-phosphine complex. A band representative of the μ-CO, observed in the X-ray structure of **6-IMes** and expected at ca. 1860 cm^{-1}, was not clearly discernible. A broad band at ~1862 cm^{-1} of very low intensity could indicate a small amount of the μ-NO isomer; however, the major NO species is indicated as a terminal NO by the relatively intense 1782 cm^{-1} band (see Figure S3, Supporting Information).

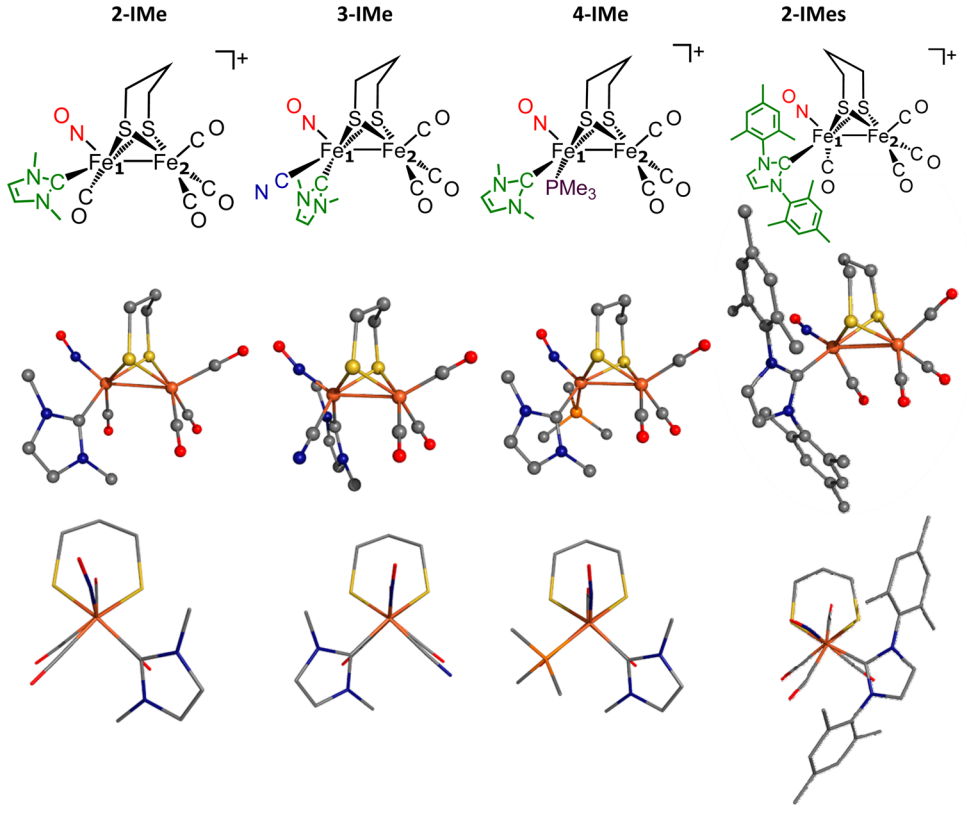

Figure 4. Molecular structures of **2-IMe**, **3-IMe**, **4-IMe**, and **2-IMes** from X-ray diffraction analysis with side view (ball-and-stick rendition) and end view (capped stick rendition). Thermal ellipsoid renderings of structures may be seen in Figures S4–S7 (Supporting Information). Hydrogen atoms, BF_4^- counterion (**2-IMe**, **4-IMe**, and **2-IMes**), and CH_2Cl_2 packing solvent (**4-IMe**) have been omitted for clarity. In all cases Fe_1 refers to the more substituted Fe; Fe_2 refers to the all-CO side.

DOI: 10.1021/acs.inorgchem.5b00072
Inorg. Chem. 2015, 54, 3523–3535

Molecular Structures of 2-IMe, 2-IMes, 3-IMe, 4-IMe, and 6-IMes from X-ray Crystallography. Crystals of **2-IMe**, **2-IMes**, **3-IMe**, **4-IMe**, and **6-IMes** were subjected to X-ray diffraction analysis, and the structures obtained are shown in Figures 4 and 5, with relevant metric parameters shown in

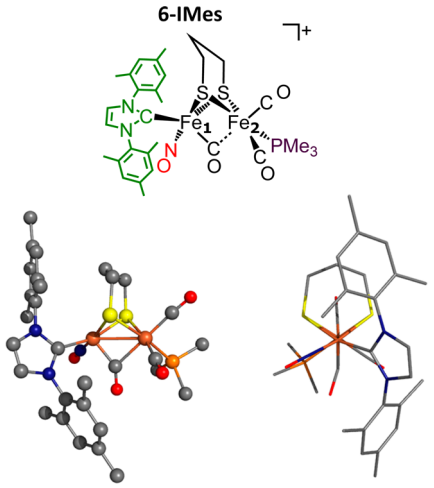

Figure 5. Molecular structure of **6-IMes** from X-ray diffraction analysis with side view (top: ball-and-stick rendition) and end view (bottom: capped stick rendition). Thermal ellipsoid rendering of this structure may be seen in Figure S8 (Supporting Information). Hydrogen atoms and BF_4^- counterion have been omitted for clarity.

Table 2. The boat conformation of the FeS_2C_3 ring is on the $Fe(CO)_3$ side of the diiron construct in **2-IMe**, **3-IMe**, and **4-IMe**. The substituted iron, Fe_1, has a slightly bent ($\angle Fe_1-N-O \approx 165°$) apical NO ligand within the $S_2Fe(NO)(NHC)(CO)$ square pyramid, shown in Figure 4.

The basal ligands of Fe_1 include both the carbene, IMe or IMes, and the differentiating ligand: CO (**2-IMe** and **2-IMes**), CN (**3-IMe**), or PMe_3 (**4-IMe**). All four complexes display the typical edge-bridged bi-square pyramidal geometry of the (μ-SRS)$[Fe_2(CO)_x(L)_{6-x}]$ family. The $N_{ap}-Fe_1-Fe_2-C_{ap}$ torsion angles of the three compounds bearing the IMe ligand are between 0.7° and 11.6°, while the analogous angle of **2-IMes** is much larger, at 55.6°. This difference in the structure of **2-IMes** may be attributed to the distortion of the Fe_1 from square pyramidal; its τ value is 0.73 (τ = 1 for trigonal bipyramid; τ = 0, square pyramid).[52] The other three structures are more regular square pyramids, with τ values ranging from 0.10 to 0.22.

The $Fe_2(CO)_3$ moieties of **2-IMe**, **3-IMe**, and **4-IMe** are nearly perfect square pyramids (τ = 0.02–0.04); again, the **2-IMes** shows more distortion, τ = 0.15. The substituted Fe_1 is displaced further out of the S_2L_2 plane, up to 0.1 Å, when compared to the Fe_2 for **2-IMe** (S_2L_2 iron displacements of Fe_1 = 0.448 Å and Fe_2 = 0.348 Å) and **3-IMe** (S_2L_2 iron displacements of Fe_1 = 0.470 Å and Fe_2 = 0.383 Å), although **4-IMe** shows less difference (S_2L_2 iron displacements of Fe_1 = 0.396 Å and Fe_2 = 0.347 Å). There is a subtle elongation of the Fe–Fe bond, from 2.543(2) and 2.568(2) Å for **2-IMe** and **3-IMe** to 2.597(1) and 2.6059(5) Å for **2-IMes** and **4-IMe**, which may be attributed to the steric effects of the larger IMes and PMe_3 ligands. Unlike the four structures above, the square pyramid of Fe_1 in the structure of **6-IMes** (Figure 5) is rotated such that the carbonyl ligand bridges Fe_1 and Fe_2. This rotated structure, analogous to the structure of **5-IMes**$^+$, has an elongated Fe_1-Fe_2 distance of 2.619(2) Å, with the μ-CO bent under the Fe_1-Fe_2 vector at an $\angle Fe_1-C-O$ of 136°. The NO ligand is in a basal position and the $\angle Fe_1-N-O$ is 175.4(6)°, in contrast to the apical NO of complexes **2-IMe**, **3-IMe**, **4-IMe**, and **2-IMes** with $\angle Fe_1-N-O$ roughly 165°.

Regioselective ^{13}CO Substitution of 2-IMe. As noted above, the decomposition of **2-IMe** in CH_2Cl_2 at 22 °C, which readily occurs even in the dark under a N_2 or Ar atmosphere, is substantially repressed under a CO atmosphere, maintaining integrity over a 24 h period; **2-IMe** is completely stable under

Table 2. Experimental Structure Metric Parameters of Compounds 2-IMe, 3-IMe, 4-IMe, 2-IMes, and 6-IMes

	2-IMe	3-IMe	4-IMe[a]	2-IMes	6-IMes
Fe_1-Fe_2	2.543(2) Å	2.568(2) Å	2.6059(5) Å	2.597(1) Å	2.619(2) Å
$Fe_1-C(NHC)$	1.995(4)	2.017(4)	2.017(3)	2.033(5)	1.986(6)
$Fe_1-N(NO)$	1.655(4)	1.672(4)	1.651(3)	1.662(5)	1.796(8)
$Fe-S^b$	2.247(3)	2.260(2)	2.250(1)	2.251(2)	2.325(2)
$Fe_1-C(CO)$	1.846(5)			1.831(6)	1.986(6)
$Fe_2-C(CO)^b$	1.797(5)	1.803(5)	1.800(4)	1.798(7)	1.790(7)
$Fe_1-C(CN)$		1.955(6)			
Fe–P(PMe3)			2.299(1)		2.275(2)
Fe_1-N-O	165.7(3)	166.4(4)	166.1(3)	163.5(5)	175.4(6)
Fe_1-C-O	177.9(4)			168.8(5)	136.1(4)
Fe_2-C-O^b	178.6(4)	178.6(4)	177.3(4)	177.7(6)	177.7(6)
$Fe-S-Fe^b$	69.4(4)	69.14(4)	70.77(3)	70.45(4)	68.56(6)
$S-Fe-S^b$	85.65(4)	85.62(4)	85.63(3)	84.54(5)	85.32(7)
N–Fe–Fe–C	11.8(4)	7.0(4)	0.7(3)	55.6(4)	
τ values[c]					
Fe_1	0.15	0.10	0.22	0.73	0.13
Fe_2	0.02	0.02	0.04	0.15	0.01
Fe displacement[d]					
Fe_1	0.448 Å	0.470 Å	0.396 Å		0.217 Å
Fe_2	0.348	0.383	0.347	0.259	0.145

[a]Values reported are average of 3 distinct molecules within the unit cell. Error is also averaged. [b]Average values and errors reported. [c]Ref 52. [d]Taken as distance of Fe from best square plane in each FeS_2L_3 square pyramid.

DOI: 10.1021/acs.inorgchem.5b00072
Inorg. Chem. 2015, 54, 3523–3535

CO or N_2 at 0 °C. To further test for CO lability, a solution of **2-IMe** in CH_2Cl_2 was placed under a blanket of ^{13}CO and held at 0 °C, observing no change in the IR spectrum. When allowed to warm to room temperature, the spectrum changed within minutes, under dark or light conditions. The ν(CO) band at 2058 cm^{-1} decreased in intensity with a concomitant growth of a new band at 2023 cm^{-1} (Figure 6). At the same time, the CO

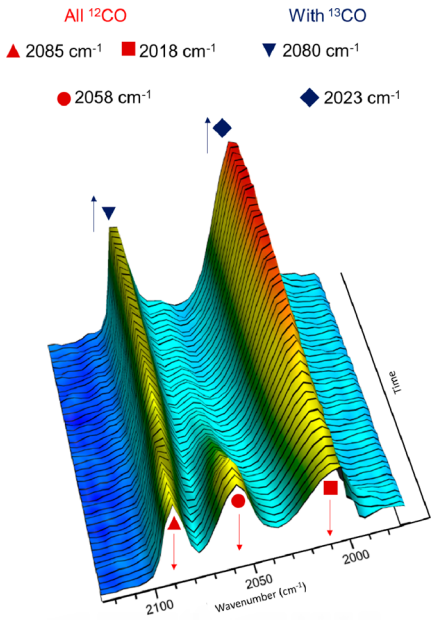

Figure 6. Three-dimensional stacked plot of the reaction of **2-IMe** with ^{13}CO(g) at 22 °C in CH_2Cl_2 showing the three CO bands of the all-^{12}CO spectrum (red shapes) shifting to the two-band pattern of the selectively substituted complex.

stretch at 2085 cm^{-1} was seen to shift only 5 cm^{-1}, to 2080 cm^{-1}, while the band at 2018 cm^{-1} overlapped with the growing band at 2023 cm^{-1} and no shift in the IR frequency could be observed.

The lone carbonyl of the Fe(IMe)(NO)(CO) moiety is, according to calculations, primarily associated with the band at 2058 cm^{-1} that changes dramatically while the two bands at 2085 and 2018 cm^{-1}, strongly associated with the $Fe_2(CO)_3$ unit, are minimally affected, indicating that the ^{13}CO substitution is site selective, exchanging exclusively with the $Fe_1(CO)$. The position shift is as expected, since the $^{12}CO/^{13}CO$ exchange of a single, uncoupled carbonyl ligand at 2058 cm^{-1} is predicted by the ratio of reduced masses of a single, uncoupled CO to shift to 2012 cm^{-1}.

The $^{12}CO/^{13}CO$ exchange reaction was monitored by *in situ* IR spectroscopy and found to have a half-life of 22 min at 22 °C in CH_2Cl_2; the rates are provided in Figure 7. The labeling of the single $Fe_1(CO)$ of **2-IMe** is effectively complete in 2 h. At this point, the system was purged with argon and the atmosphere was replaced with ^{12}CO. The reverse reaction, substitution of the ^{12}CO for the single ^{13}CO, occurs cleanly, regenerating the all-^{12}CO IR spectrum at the same rate (Figure 7, Figures S9 and S10, Supporting Information).

NMR Studies. The photodissociation of carbon monoxide from (μ-pdt)[$Fe(CO)_3$]$_2$ is a well-known method for promoting $^{12}CO/^{13}CO$ exchange for ^{13}C NMR studies.[1] The thus-obtained ^{13}CO-labeled complex was used as the precursor to synthesize **2-IMe** in which all CO ligands are equally

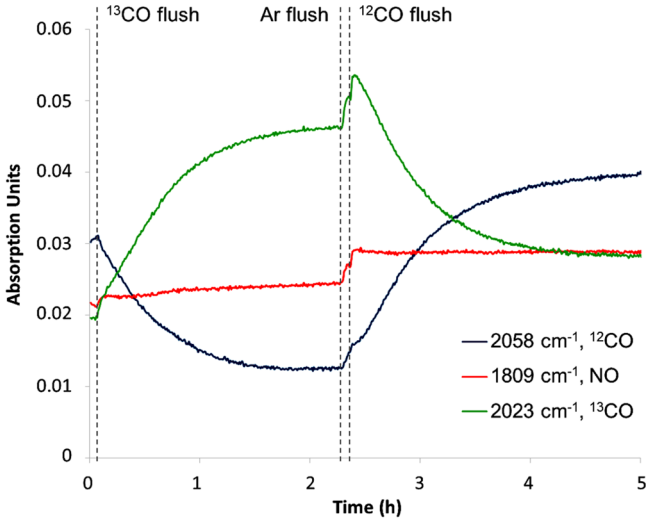

Species	k_{obs} (x 10^4 s^{-1})
2023 cm^{-1}, ^{13}CO ↑	5.32
2058 cm^{-1}, ^{12}CO ↓	-5.59
2058 cm^{-1}, ^{12}CO ↑	5.01
2023 cm^{-1}, ^{13}CO ↓	-5.42

Figure 7. Top is the reaction profile of IR bands corresponding to the ^{12}CO at 2058 cm^{-1} (blue), the ^{13}CO at 2023 cm^{-1} (green), and the NO at 1809 cm^{-1} (red). The vertical lines show the times when ^{13}CO, argon, and ^{12}CO were flushed into the solution of **2-IMe**. Below are the observed rate constants obtained from linear natural log plots taken over 2−3 half-lives.

enriched. The ^{13}C NMR spectrum of this complex at 0 °C reveals four resonances in the CO region as all four carbonyls are in distinct electronic environments, including the two basal carbonyls of the $Fe(CO)_3$ unit, which are distinguished as being *transoid* or *cisoid* to the NHC on the opposite iron (Figure 8A).

The ^{13}C NMR spectroscopy of **1**, (μ-pdt)[$Fe(CO)_3$]$_2$, has been investigated extensively.[1,53] At low temperature (−80 °C), four resonances are seen in the low field CO region, with the two apical and two pairs of basal COs distinguished by the locked bridgehead position of the dithiolate. Upon warming, coalescence is seen at −60 °C, and by −20 °C, a single resonance is observed, assigned to the carbonyls of the $Fe(CO)_3$ units which are in rapid intramolecular exchange on individual iron centers, concurrent with rapid equilibration of the bridgehead CH_2 unit of the pdt. In contrast, on warming a sample of **2-IMe** to 30 °C, no change is observed in the positions of the resonances, although the three peaks ultimately assigned to the $Fe(CO)_3$ carbonyls broaden slightly (Figure S11, Supporting Information). Due to the thermal instability of **2-IMe**, the coalescence temperature could not be measured, and therefore, the experimental rotational barrier could not be determined.

The $^{12}CO/^{13}CO$ exchange of the single carbonyl of the Fe(IMe)(NO)(CO) moiety was also monitored by ^{13}C NMR spectroscopy. The low field CO region of a sample of **2-IMe** that had been exposed to ^{13}CO at 22 °C for 2 h shows the same four resonances as above, but the peak at 207.1 ppm is much more intense (Figure 8B) and hence assigned to the unique CO, the $Fe_1(CO)$. Integration of the resonances shows a ∼15:1

DOI: 10.1021/acs.inorgchem.5b00072
Inorg. Chem. 2015, 54, 3523−3535

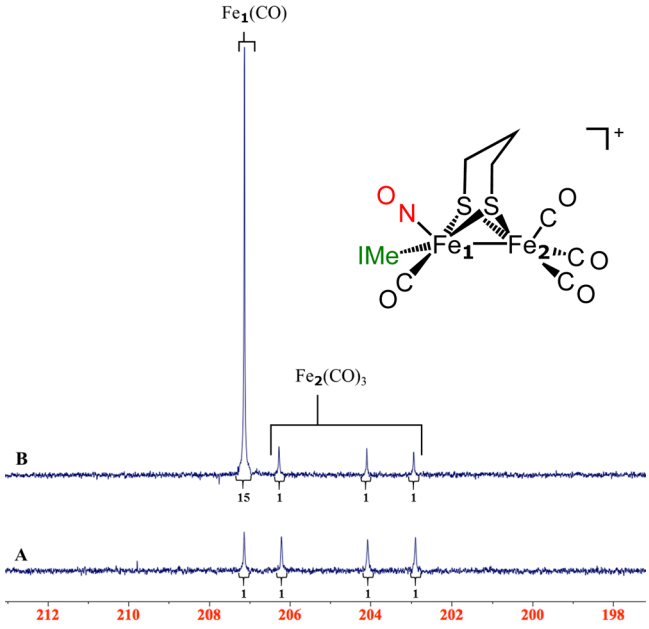

Figure 8. Low-field ^{13}C NMR spectra in CD_2Cl_2 at 0 °C of (A) a sample of **2-IMe** synthesized from ^{13}CO enriched **1** and (B) a sample of **2-IMe** synthesized from all-^{12}CO **1**, after 2 h under 1 atm of ^{13}CO. The peak at 207.1 ppm is ~15 times the intensity of the three peaks at 206.2, 204.0, and 202.9 ppm.

ratio of ^{13}CO that has been exchanged for the $Fe_1(CO)$ relative to the $Fe_2(CO)_3$ carbonyls.

In a similar fashion to the experiment above, a solution of complex **2-IMe** in CD_2Cl_2 was placed under a blanket of ^{13}CO at 22 °C, and the $^{12}CO/^{13}CO$ exchange was monitored with aliquots removed at 10 min time intervals and flash-frozen under N_2. Consistent with our conclusions above, the ^{13}C NMR spectra of these samples show increases in the intensity of the $Fe_1(CO)$ relative to the intensity of the three carbonyls assigned to the $Fe_2(CO)_3$, from a 1:1 ratio at 0 min to 19:1 at 30 min, with intermediate ratios of 10:1 and 16:1 at 10 and 20 min, respectively (Figure S12, Supporting Information). This indicates that, if the $Fe_2(CO)_3$ also exchanges bound ^{12}CO with the ^{13}CO atmosphere in the reaction flask, it is at a much slower rate.

A second route for $^{12}CO/^{13}CO$ exchange into the $Fe_2(CO)_3$ unit would be by intramolecular site exchange with ^{13}CO on the $Fe_1(^{13}CO)$. To test this possibility, a sample of regioselectively singly labeled **2-IMe** was allowed to equilibrate under N_2 in the NMR tube, held at 22 °C. The relative ratio of intensities of the ^{13}C resonances assigned to each iron decreases from 14:1:1:1 to 9:1:1:1 over 2 h (Figure S13, Supporting Information). When referenced to the CD_2Cl_2 resonance, the CO band assigned to the $Fe_1(CO)$ decreases while the CO bands assigned to the $Fe_2(CO)_3$ increase. Hence, a very slow CO exchange between the two irons appears to be occurring.

Density Functional Theory Investigations of Structural Isomer Stability of 2-IMe and 4-IMe. In order to gain insight into the structures of **2-IMe** and **4-IMe**, a series of isomers of formula (μ-pdt)$[Fe_2(CO)_3(NO)(IMe)(L)]^+$, L = CO (**2-IMe**) and PMe_3 (**4-IMe**), were optimized using the B3LYP functional[43−45] with the 6-311+G(d,p) basis set[46,47] on all atoms. In Charts 1−3, the calculated free energies are reported relative to the isomer corresponding to the X-ray

Chart 1. Calculated Energies of All-Terminal Isomers of (μ-pdt)$[Fe_2(CO)_4(NO)(IMe)]^+$, Relative to 2-IMe-1, the Structure Corresponding to 2-IMe

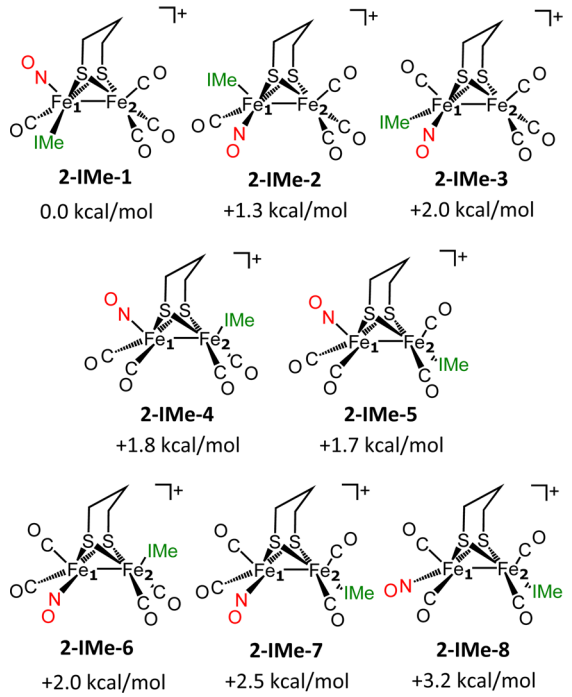

crystal structure of each. From this data, we conclude that the isomer observed in the solid state structure of **2-IMe** is thermodynamically favored (Chart 1).

All possible permutations of the formula (μ-pdt)$[Fe_2(CO)_4(NO)(IMe)]^+$, in which the bridging propane dithiolate ligand is positioned away from the $Fe_1(NO)$, are displayed in Chart 1. All energies are reported relative to the structure corresponding to the X-ray crystal structure, **2-IMe-1**. The isomer resulting from positioning the IMe ligand apical (**2-IMe-2**) or CO apical (**2-IMe-3**) is less stable than **2-IMe-1** by 1.3 and 2.0 kcal/mol, respectively. Isomers resulting from moving the IMe ligand onto Fe_2 in either the apical (**2-IMe-4**) or the basal (**2-IMe-5**) position are also higher in energy, by 1.8 and 1.7 kcal/mol, respectively. Three additional isomers are available where the NO and IMe are on individual irons with the NO in the basal position, but all are less stable than **2-IMe-1** by 2.0 (**2-IMe-6**), 2.5 (**2-IMe-7**), and 3.2 (**2-IMe-8**) kcal/mol. The minor differences in energy of these calculated structures speak to the inherent electronic flexibility of the 2Fe unit. Generally, one can conclude that NO prefers the apical site on the same Fe as the better donor.

When on the same Fe, the good donor properties of the NHC ligand are overwhelmed by the exceptional accepting ability of NO^+. The latter creates a dearth of π-density available from the iron for backbonding to the CO of **2-NHC**, resulting in a labile CO ligand on Fe_1, as observed by the increased Fe_1−CO bond distances of **2-IMe** and **2-IMes** and demonstrated by regioselective CO exchange with added ^{13}CO. As CO is a poor nucleophile, our expectation is that this exchange occurs via a dissociative path. Phosphine exchange is also regioselective at the same site, in a very rapid (time of mixing) reaction, generating a stable **4-IMe**. Because the rate of the PMe_3/CO exchange is so much greater than that of the $^{12}CO/^{13}CO$ exchange, it is likely that the combination of good nucleophilicity of the PMe_3 and the good electrophilicity of

DOI: 10.1021/acs.inorgchem.5b00072
Inorg. Chem. 2015, 54, 3523−3535

the Fe to which an NO is attached drives the reaction toward an associative interchange mechanism. The speed of this PMe_3 reaction has prevented detailed kinetic studies.

A second question asked of the computations addressed the nature of the transition state for $Fe(CO)_3$ rotation (Chart 2).

Chart 2. Calculated Energies of Rotated Structures of (μ-pdt)[Fe_1(IMe)(NO)(CO)][$Fe_2(CO)_3$]$^+$ Relative to 2-IMe-1, Consisting of Four Transition States and One Ground State Isomer, 2-IMe-13

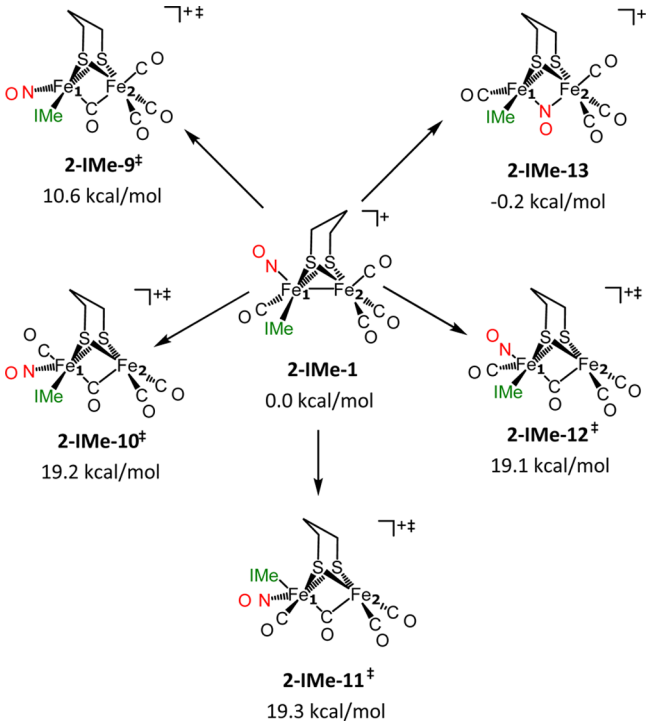

The calculations indicated that the rotation of the $Fe(CO)_3$ unit of **2-IMe** has an energy barrier (19.1−19.3 kcal/mol) that is much higher than that of **1** (11.6 kcal/mol), regardless of the ligand *trans* to the semibridging CO. This high barrier to rotation gains experimental support from the ^{13}C NMR spectroscopy, which revealed that the $Fe(CO)_3$ carbonyls are not exchanging at temperatures as high as 30 °C. In contrast, the rotation of the Fe(IMe)(NO)(CO) moiety has a single bridging CO structure, **2-IMe-9‡**, at 10.6 kcal/mol, which is lower in energy than the calculated rotation barrier of **1**. Attempts to locate a transition state with the NO in a bridging position were unsuccessful; however, a structure with the bridging NO was located as a stable isomer, **2-IMe-13**, which was 0.2 kcal/mol more stable than **2-IMe-1**. This isomer would be expected to have a bridging ν(NO) band near 1500 cm^{-1} and has not been observed experimentally; furthermore, DFT calculations utilizing pure functionals suggest that the μ-NO isomer is significantly higher in energy than the all-terminal isomer.

The resistance of the $Fe(CO)_3$ unit in **2-IMe** to undergo intramolecular CO site exchange via the turnstile rotation that leads to the inverted square pyramid arrangement, which is typical of the (μ-SRS)[$Fe(CO)_3$]$_2$ complexes, is a curiosity. We posit that the cause of this large exchange barrier is, in fact, related to the geometrical differences of **6-NHC** vs **4-NHC** in Scheme 1. The computations suggest that rotations, producing a bridging CO, are only likely when the μ-CO originates from the electron-deficient side, and that the μ-CO requires stabilization by an Fe → CO (iron d-orbital to CO π^*) interaction that delocalizes excess charge from the electron-rich Fe to the relatively electron-poor Fe. This interaction lowers the activation barrier to rotation and, in cases where the drive to equalize charge asymmetry is assisted by appropriate steric bulk, may even yield a stable rotated structure.

The resistance to rotation of **2-IMe** is, therefore, attributed to the electron-withdrawing nitrosyl ligand and its depletion of the π-density on Fe_1 that might have been used to stabilize a μ-bridging CO originating from Fe_2. This is corroborated by the increased Fe_1-C_{br} distance of the calculated rotated structures of **2-IMe** and analogous values derived from a series of simpler models (μ-pdt)[$Fe(CO)_2NO$][$Fe(CO)_3$]$^+$ (**1-NO$^+$**), (μ-pdt)-[$Fe(CO)_3$]$_2$ (**1**), and (pdt)[$Fe(CO)_2CN$][$Fe(CO)_3$]$^-$ (**1-CN$^-$**) that we have computed to further test the conclusions above (Figure 9). The table within Figure 9 lists the calculated ΔG_{act} of the rotation of $Fe_2(CO)_3$ in comparison to the Fe−Fe distances of the calculated ground and transition state structures, calculated atomic polar tensor (APT) charges of the μ-CO, and Fe_1-C_{br} distances of the transition state structures. The best correlation is found in the calculated increase in the Fe−Fe distance from the ground state to transition state structures (Δ[Fe_1-Fe_2]), as the Fe−Fe bond must open up as the decreasing electron density on Fe_1 lessens its ability to stabilize the μ-CO. In addition, the barrier to rotation inversely correlates with the charge on the bridging or semibridging carbonyl ligand, which becomes more negative as the donation from the Fe_1 increases. These data show that the rotational barrier of such $Fe(CO)_3$ units is heavily influenced by the stabilizing interaction of the Fe_1 to the $Fe_2(CO)_3$.

A further computational investigation compared the stability of complexes **4-IMe** and **6-IMe**. As both isomers have been synthesized, through different routes, we queried which is the thermodynamic product. In the same manner as the study of **2-IMe** above, the investigation of the isomers of **4-IMe** was performed with the free energy of various isomers of (μ-pdt)[$Fe_2(CO)_3$(NO)(IMe)(PMe_3)]$^+$ reported relative to the isomer corresponding to the X-ray crystal structure of **4-IMe**, **4-IMe-1** (Chart 3). Moving the PMe_3 ligand onto Fe_2, **4-IMe-2**, results in greater stability than the fully dissymmetric **4-IMe-1**, by 3.6 kcal/mol. An even lower energy isomer, obtained by the rotation of the Fe_1, resulting in a bridging CO, **4-IMe-3**, is more stable than **4-IMe-1** by 5.0 kcal/mol. This isomer corresponds to the X-ray structure of **6-IMes** *sans* the bulky mesityl groups on the carbene. Another rotated isomer, although synthetically inaccessible, is a more stable arrangement for a rotated μ-CO structure (at −9.0 kcal/mol) that places the PMe_3 and NO^+ on the Fe_1 rotated side, allowing the Fe_2, which is equipped with the better donating NHC ligand, to serve as donor to the μ-CO bridge, generating **4-IMe-4**.

CONCLUSION

The regioselectivity demonstrated by the ligand substitutions in thiolate-bridged diiron complexes as described above point to communication between the irons that affects both ground state and transition state structural forms. From our studies[26] and earlier ones of Rauchfuss et al.,[24,25] we conclude that the installment of an electrophilic ligand, NO^+, on the diiron platform via isoelectronic NO^+/CO exchange can only occur if the parent (μ-pdt)[$Fe(CO)_3$]$_2$, **1**, has enhancement of electron density through a prior nucleophilic ligand exchange as in (μ-pdt)[$Fe(CO)_2$NHC][$Fe(CO)_3$], **1-NHC**. The NO^+ then adds

DOI: 10.1021/acs.inorgchem.5b00072
Inorg. Chem. 2015, 54, 3523−3535

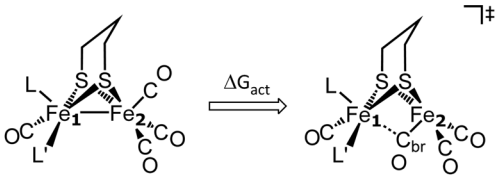

L	L'	ΔG_{act} (kcal/mol)	Fe_1-Fe_2 (Å)	$[Fe_1$-$Fe_2]^{\ddagger}$ (Å)	$\Delta[Fe_1$-$Fe_2]^{a}$ (Å)	(μ-CO) charge	$[Fe_1$-$C_{br}]^{\ddagger}$ (Å)
CN^-	CO	5.0	2.558	2.587	0.029	0.239	2.339
CO	CO	11.6	2.530	2.601	0.071	0.285	2.200
NO^+	CO	17.6	2.601	2.725	0.124	0.439	3.011
NO^+	NHC	19.1	2.601	2.742	0.141	0.421	3.118

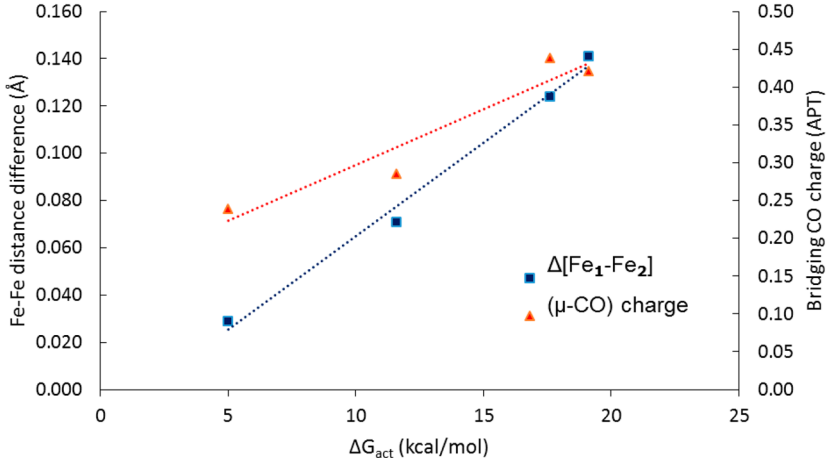

Figure 9. Increase in $\Delta[Fe_1{-}Fe_2]$ (given as the difference of the $Fe_1{-}Fe_2$ distances of the calculated transition state and ground state structures) and decrease in the charge of the bridging carbonyl (calculated by APT) show a linear correlation (R^2 values of 0.99 and 0.92, respectively) with the rotation barrier of the $Fe_2(CO)_3$ in a series of complexes that vary in the CO substitution of Fe_1: **1-CN⁻**, **1**, **1-NO⁺**, and **2-IMe**. These trends illustrate the effect of the π electron density of Fe_1, as modulated by CO/L substitution, on the rotation barrier of the $Fe_2(CO)_3$.

Chart 3. Calculated Energies of Selected Isomers of $(\mu\text{-pdt})[Fe_2(CO)_3(NO)(IMe)(PMe_3)]^+$, a Comparison of the Stability of 4-NHC (4-IMe-1) and 6-NHC (4-IMe-3) Relative to 4-IMe-1

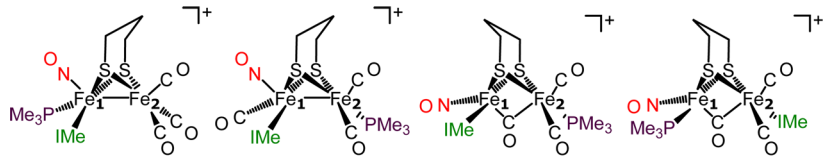

4-IMe-1 0.0 kcal/mol
4-IMe-2 -3.6 kcal/mol
4-IMe-3 -5.0 kcal/mol
4-IMe-4 -9.0 kcal/mol

to the more electron-rich side, displacing CO and yielding one regioisomer, $(\mu\text{-pdt})[Fe(NHC)(NO)(CO)][Fe(CO)_3]^+$, **2-NHC**. To this complex another strong nucleophile, CN^- or PMe_3, will be directed and trapped on the nitrosylated iron, yielding $(\mu\text{-pdt})[Fe(NHC)(NO)(CN)][Fe(CO)_3]$, **3-NHC**, and $(\mu\text{-pdt})[Fe(NHC)(NO)PMe_3][Fe(CO)_3]^+$, **4-NHC**, respectively. An alternative order of addition, PMe_3 before NO^+ to **1-NHC**, first produces the mixed ligand complex $(\mu\text{-pdt})[Fe(CO)_2NHC][Fe(CO)_2PMe_3]$, **5-NHC**. Subsequent NO^+/CO exchange is directed to the iron bound to the better electron-donating NHC ligand, yielding $(\mu\text{-pdt})(\mu\text{-CO})[Fe(NHC)(NO)][Fe(CO)_2PMe_3]^+$, **6-NHC**, which is both a regio- and a structural isomer of **4-NHC** (Scheme 1).

In summary, the electronic asymmetry in the diiron complexes resulting from NO^+/CO exchange has major effects: it induces the rotation of Fe_1 in **6-IMes**, as Fe_1 is the more electrophilic and has a CO that can shift into the bridging position where it is stabilized by the interaction of Fe_2, the latter made electron-rich by the single PMe_3 ligand. In contrast, the $Fe_2(CO)_3$ rotation in **4-IMe** is retarded as, in the presence of one or even two good donor ligands on Fe_1, the overriding electron-withdrawing ability of NO^+ prevents Fe_1 donation to a potential μ-CO from Fe_2. Our complex **6-IMes** (Figure 5) with the "rotated" geometry and μ-CO ligand is obviously the structural mimic of the 2Fe subsite within the [FeFe]-H_2ase (Figure 1) with the distal Fe (Fe_d, the iron furthest from the 4Fe4S cluster and in the rotated form with only one good donor ligand, CN^-) related to the Fe_1 of **6-IMes**. The proximal Fe (Fe_p) in the active site has two good donor ligands, a CN^- and a [4Fe4S]-thiolate sulfur, producing an electron-rich iron that relates to Fe_2 of **6-IMes**. The electronic asymmetry that is required for the isomeric form of the diiron complex expected to be optimal for the catalysis can be achieved by first coordination sphere ligand arrangements that tilt the balance of electrophilicity/nucleophilicity at each iron in a manner interpretable by conventional tenets of organometallic chemistry.

DOI: 10.1021/acs.inorgchem.5b00072
Inorg. Chem. 2015, 54, 3523−3535

Clearly the role of H-bonding to cyanide within the enzyme active site cavity and the influence of the second coordination sphere are additional considerations of the diiron subcluster of [FeFe]-H_2ase for the rotated geometry, which evidently is maintained throughout the electrochemical cycle. In this regard, it should be noted that steric encumbrance at the bridgehead of diiron biomimetics may induce the rotated geometry even in the Fe^IFe^I redox level.[26,54]

■ ASSOCIATED CONTENT

Supporting Information

Cyclic voltammetry of **2-IMes** and **4-IMe**; FTIR spectra of **1-IMe**, **1-IMes**, **2-IMe**, **2-IMes**, **5-IMes**, **5-IMes**$^+$, and **6-IMes**; X-ray crystallographic data, ORTEPs, and Cartesian coordinates for **2-IMe**, **2-IMes**, **3-IMe**, **4-IMe**, and **6-IMes**; kinetic analyses by *in situ* FTIR spectroscopy; ^{13}C NMR spectroscopy of **2-IMe**; and coordinates for the calculated isomers of **2-IMe** and **4-IMe**. This material is available free of charge via the Internet at http://pubs.acs.org.

■ AUTHOR INFORMATION

Corresponding Authors

*E-mail: hall@chem.tamu.edu (M.B.H.).

*E-mail: marcetta@mail.chem.tamu.edu (M.Y.D.).

Notes

The authors declare no competing financial interest.

■ ACKNOWLEDGMENTS

We are grateful for the financial support from the National Science Foundation (CHE-1266097 to M.Y.D., CHE-1300787 to M.B.H.) and the R. A. Welch Foundation (A-0924 to M.Y.D., A-0648 to M.B.H.). We thank Dr. Nattamai Bhuvanesh for refining the disorder in the crystallographic structures and Sam Kyran from the Donald J. Darensbourg group for the ReactIR and kinetics measurements.

■ REFERENCES

(1) (a) Winter, A.; Zsolnai, L.; Huttner, G. *Z. Naturforsch.* **1982**, *37b*, 1430−1436. (b) Lyon, E. J.; Georgakaki, I. P.; Reibenspies, J. H.; Darensbourg, M. Y. *J. Am. Chem. Soc.* **2001**, *123*, 3268−3278.

(2) Nicolet, Y.; Lemon, B. J.; Fontecilla-Camps, J. C.; Peters, J. W. *Trends Biochem. Sci.* **2000**, *25*, 138−143.

(3) Felton, G. A. N.; Mebi, C. A.; Petro, B. J.; Vannucci, A. K.; Evans, D. H.; Glass, R. S.; Lichtenberger, D. L. *J. Organomet. Chem.* **2009**, *694*, 2681−2699.

(4) Gloaguen, F.; Rauchfuss, T. B. *Chem. Soc. Rev.* **2009**, *38*, 100−108.

(5) Tard, C.; Pickett, C. J. *Chem. Rev.* **2009**, *109*, 1145−1174.

(6) Lubitz, W.; Ogata, H.; Ruediger, O.; Reijerse, E. *Chem. Rev.* **2014**, *114*, 4081−4148.

(7) Li, Y.; Zhong, W.; Qian, G.; Xiao, Z.; Liu, X. *Appl. Organomet. Chem.* **2013**, *27*, 253−260.

(8) Heine, D.; Pietsch, C.; Schubert, U. S.; Weigand, W. *J. Polym. Sci.* **2013**, *51*, 2171−2180.

(9) Pullen, S.; Fei, H.; Orthaber, A.; Cohen, S. M.; Ott, S. *J. Am. Chem. Soc.* **2013**, *135*, 16997−7003.

(10) Berggren, G.; Adamska, A.; Lambertz, C.; Simmons, T. R.; Esselborn, J.; Atta, M.; Gambarelli, S.; Mouesca, J. M.; Reijerse, E.; Lubitz, W.; Happe, T.; Artero, V.; Fontecave, M. *Nature* **2013**, *499*, 66−69.

(11) Esselborn, J.; Lambertz, C.; Adamska-Venkatesh, A.; Simmons, T.; Berggren, G.; Noth, J.; Siebel, J.; Hemschemeier, A.; Artero, V.; Reijerse, E.; Fontecave, M.; Lubitz, W.; Happe, T. *Nat. Chem. Bio.* **2013**, *9*, 607−609.

(12) Mulder, D. W.; Boyd, E. S.; Sarma, R.; Lange, R. K.; Endrizzi, J. A.; Broderick, J. B.; Peters, J. W. *Nature* **2010**, *465*, 248−251.

(13) Nicolet, Y.; Piras, C.; Legrand, P.; Hatchikian, C. E.; Fontecilla-Camps, J. C. *Structure* **1999**, *7*, 13−23.

(14) Stanley, J. L.; Rauchfuss, T. B.; Wilson, S. R. *Organometallics* **2007**, *26*, 1907−1911.

(15) Darensbourg, M. Y.; Lyon, E. J.; Zhao, X.; Georgakaki, I. P. *Proc. Nat. Acad. Sci. U.S.A.* **2003**, *100*, 3683−3688.

(16) George, S. J.; Cui, Z.; Razavet, M.; Pickett, C. J. *Chem.—Eur. J.* **2002**, *8*, 4037−4046.

(17) Mulder, D. W.; Ortillo, D. O.; Gardenghi, D. J.; Naumov, A. V.; Ruebush, S. S.; Szilagyi, R. K.; Huynh, B.; Broderick, J. B.; Peters, J. W. *Biochemistry* **2009**, *48*, 6240−6248.

(18) Bethel, R. D.; Singleton, M. L.; Darensbourg, M. Y. *Angew. Chem., Int. Ed.* **2010**, *49*, 8567−8569.

(19) Li, B.; Liu, T.; Singleton, M. L.; Darensbourg, M. Y. *Inorg. Chem.* **2009**, *48*, 8393−8403.

(20) Fauvel, K.; Mathieu, R.; Poilblanc, R. *Inorg. Chem.* **1976**, *4*, 976−978.

(21) Olsen, M. T.; Gray, D. L.; Rauchfuss, T. B.; Gioia, L. D.; Zampella, G. *Chem. Commun.* **2011**, *47*, 6554−6556.

(22) Tye, J. W.; Darensbourg, M. Y.; Hall, M. B. *J. Mol. Struct.: THEOCHEM* **2006**, *771*, 123−128.

(23) Zhao, X.; Chiang, C. Y.; Miller, M. L.; Rampersad, M. V.; Darensbourg, M. Y. *J. Am. Chem. Soc.* **2003**, *125*, 518−524.

(24) Zaffaroni, R.; Rauchfuss, T. B.; Gray, D. L.; De Gioia, L.; Zampella, G. *J. Am. Chem. Soc.* **2012**, *134*, 19260−19269.

(25) (a) Olsen, M. T.; Bruschi, M.; De Gioia, L.; Rauchfuss, T. B.; Wilson, S. R. *J. Am. Chem. Soc.* **2008**, *130*, 12021−12030. (b) Olsen, M. T.; Justice, A. K.; Gloaguen, F.; Rauchfuss, T. B.; Wilson, S. R. *Inorg. Chem.* **2008**, *47*, 11816−11824.

(26) Hsieh, C. H.; Erdem, O. F.; Harman, S. D.; Singleton, M. L.; Reijerse, E.; Lubitz, W.; Popescu, C. V.; Reibenspies, J. H.; Brothers, S. M.; Hall, M. B.; Darensbourg, M. Y. *J. Am. Chem. Soc.* **2012**, *134*, 13089−13102.

(27) Lin, J. T.; Huang, P. S.; Tsai, T. Y. R.; Liao, C.; Tseng, L.-H.; Wen, Y. S.; Shi, F.-K. *Inorg. Chem.* **1992**, *31*, 4444−4452.

(28) Enemark, J. H.; Feltham, R. D. *Coord. Chem. Rev.* **1974**, *13*, 339−406.

(29) Liu, T.; Darensbourg, M. Y. *J. Am. Chem. Soc.* **2007**, *129*, 7008−7009.

(30) Arduengo, A. J., III; Dias, H. V. R.; Harlow, R. L.; Kline, M. *J. Am. Chem. Soc.* **1992**, *114*, 5530.

(31) Bantreil, X.; Nolan, S. P. *Nat. Protoc.* **2011**, *6*, 69−77.

(32) Capon, J.-F.; El Hassnaoui, S.; Gloaguen, F.; Schollhammer, P.; Talarmin, J. *Organometallics* **2005**, *24*, 2020−2022.

(33) Tye, J. W.; Lee, J.; Wang, H. W.; Mejia-Rodriguez, R.; Reibenspies, J. H.; Hall, M. B.; Darensbourg, M. Y. *Inorg. Chem.* **2005**, *44*, 5550−5552.

(34) Thomas, C. M.; Liu, T.; Hall, M. B.; Darensbourg, M. Y. *Inorg. Chem.* **2008**, *47*, 7009−7024.

(35) *APEX2*, version 2009.7-0; Bruker AXS Inc.: Madison, WI, 2007.

(36) Sheldrick, G. M. *SADABS: Program for Absorption Correction of Area Detector Frames*; Bruker AXS Inc.: Madison, WI, 2001.

(37) Sheldrick, G. M. *SHELXS-97: Program for Crystal Structure Solution*; Universität Göttingen: Göttingen, Germany, 1997.

(38) Sheldrick, G. M. *SHELXL-97: Program for Crystal Structure Refinement*; Universität Göttingen: Göttingen, Germany, 1997.

(39) Barbour, L. J. *J. Supramol. Chem.* **2003**, *1*, 189−191.

(40) Mercury; Macrae, C. F.; Edgington, P. R.; McCabe, P.; Pidcock, E.; Shields, G. P.; Taylor, R.; Towler, M.; van de Streek, J. *J. Appl. Crystallogr.* **2006**, *39*, 453−457.

(41) Farrugia, L. J. *J. Appl. Crystallogr.* **1999**, *32*, 837−838.

(42) Frisch, M. J.; Trucks, G. W.; Schlegel, H. B.; Scuseria, G. E.; Robb, M. A.; Cheeseman, J. R.; Scalmani, G.; Barone, V.; Mennucci, B.; Petersson, G. A.; Nakatsuji, H.; Caricato, M.; Li, X.; Hratchian, H. P.; Izmaylov, A. F.; Bloino, J.; Zheng, G.; Sonnenberg, J. L.; Hada, M.; Ehara, M.; Toyota, K.; Fukuda, R.; Hasegawa, J.; Ishida, M.; Nakajima, T.; Honda, Y.; Kitao, O.; Nakai, H.; Vreven, T.; Montgomery, J. A., Jr.;

DOI: 10.1021/acs.inorgchem.5b00072
Inorg. Chem. 2015, 54, 3523−3535

Peralta, J. E.; Ogliaro, F.; Bearpark, M.; Heyd, J. J.; Brothers, E.; Kudin, K. N.; Staroverov, V. N.; Kobayashi, R.; Normand, J.; Raghavachari, K.; Rendell, A.; Burant, J. C.; Iyengar, S. S.; Tomasi, J.; Cossi, M.; Rega, N.; Millam, N. J.; Klene, M.; Knox, J. E.; Cross, J. B.; Bakken, V.; Adamo, C.; Jaramillo, J.; Gomperts, R.; Stratmann, R. E.; Yazyev, O.; Austin, A. J.; Cammi, R.; Pomelli, C.; Ochterski, J. W.; Martin, R. L.; Morokuma, K.; Zakrzewski, V. G.; Voth, G. A.; Salvador, P.; Dannenberg, J. J.; Dapprich, S.; Daniels, A. D.; Farkas, Ö.; Foresman, J. B.; Ortiz, J. V.; Cioslowski, J.; Fox, D. J. *Gaussian 09*, Revision B.01; Gaussian, Inc.: Wallingford, CT, 2009.

(43) Becke, A. D. *J. Chem. Phys.* **1993**, *98*, 5648−5652.

(44) Stephens, P. J.; Devlin, F. J.; Chabalowski, C. F.; Frisch, M. J. *J. Phys. Chem.* **1994**, *98*, 11623−11627.

(45) Lee, C. T.; Yang, W. T.; Parr, R. G. *Phys. Rev. B* **1988**, *37*, 785−789.

(46) Krishnan, R.; Binkley, J. S.; Seeger, R.; Pople, J. A. *J. Chem. Phys.* **1980**, *72*, 650−654.

(47) McLean, A. D.; Chandler, G. S. *J. Chem. Phys.* **1980**, *72*, 5639−5648.

(48) *AMPAC 9*; Semichem, Inc.: Shawnee, KS, 1992.

(49) Connelly, N. G.; Geiger, W. E. *Chem. Rev.* **1996**, *96*, 877−910.

(50) Heo, G. S.; Hillman, P. E.; Bartsch, R. A. *J. Heterocyclic Chem.* **1982**, *19*, 1099−1103.

(51) Davison, A.; Green, M. L. H.; Wilkinson, G. *J. Chem. Soc.* **1961**, 3172−3177.

(52) Addison, A. W.; Rao, T. N.; Reedijk, J.; Van Rijn, J.; Verschoor, G. C. *J. Chem. Soc., Dalton Trans.* **1984**, 1349−1356.

(53) Crouthers, D. J.; Denny, J. A.; Bethel, R. D.; Munoz, D. G.; Darensbourg, M. Y. *Organometallics* **2014**, *33*, 4747−4755.

(54) Goy, R.; Bertini, L.; Elleouet, C.; Görls, H.; Zampella, G.; Talarmin, J.; Gioia, L. D.; Schollhammer, P.; Apfel, U.-P.; Weigand, W. *Dalton Trans.* **2015**, *44*, 1690−1699.

DOI: 10.1021/acs.inorgchem.5b00072
Inorg. Chem. 2015, 54, 3523−3535